https://doi.org/10.5194/egusphere-2026-6185
Preprint. Discussion started: 16 November 2026
© Author(s) 2026. CC BY 4.0 License.

Quantifying the Global Warming Potential of Trifluoromethyl Hypofluorite (CF_3OF): Infrared Absorption Cross-Sections and Decay Measurements

Dongkyum Kim[†,1,3,*], Hyeonbin Kim[†,2], Hyeon Ki Park[4], Sang Jeen Hong[2,*], Bumsuk Jung[1,2,*]

[1]Department of Semiconductor Equipment Engineering, Myongji University, 116 Myongji-ro, Cheoin-gu, Yongin-si, Gyeonggi-do 17058, Republic of Korea
[2]Department of Semiconductor Engineering, Myongji University, 116 Myongji-ro, Cheoin-gu, Yongin-si, Gyeonggi-do 17058, Republic of Korea
[3]DQST Corp. (DQ Science and Technology), Unit B02, Shopping Arcade, Hyoseong Sang-a Apartments, 51, Gyebaek-ro 1686beon-gil, Jung-gu, Daejeon 34957, Republic of Korea
[4] SOLE Materials Co., Ltd., 62, Hugi-gil, Ochang-eup, Cheongwon-gu, Cheongju-si, Chungcheongbuk-do 28105, Republic of Korea
*Correspondence to: Dongkyum Kim (dongkyum.kim@mju.ac.kr), Sang Jeen Hong (samhong@mju.ac.kr) and Bumsuk Jung (bjung@mju.ac.kr)
† Dongkyum Kim and Hyeonbin Kim share first authorship.

Abstract.

Trifluoromethyl hypofluorite (CF_3OF) is being investigated as an alternative gas for plasma processing, but assessment of its global warming potential (GWP) requires compound-specific measurements of infrared absorption and persistence. We measured its gas-phase infrared absorption cross-section (ACS) by Fourier transform infrared (FT-IR) spectroscopy and calculated its radiative efficiency (RE). We monitored its decay in near-anhydrous and humid gas matrices. The spectrum was dominated by the 1167–1305 cm^{-1} absorption band. Its integrated ACS over 833.5–3000 cm^{-1} was 1.25×10^{-16} cm $molecule^{-1}$, and weighting with the stratospheric-adjusted Pinnock curve yielded a mixing-ratio-based RE of 0.108 W m^{-2} ppb^{-1}. The CF_3OF e-folding decay time was 3451 min in near-anhydrous synthetic air and 2704 min in 40 % O_2/60 % Ar. In ambient air, it decreased from 2448 to 168 min as the absolute humidity increased from 3.8 to 22.2 g m^{-3}, demonstrating that water vapor strongly accelerated CF_3OF removal. In near-anhydrous synthetic air, the CO_2 rise time of 3591 min agreed with the CF_3OF decay time to within 4.1 %, supporting a kinetic association between CF_3OF loss and CO_2 formation. Using the condition-specific decay times and the mass-based RE adjusted by a lifetime-dependent atmospheric-distribution factor, we calculated direct 100-year GWP (GWP_{100}) values ranging from 3.44×10^{-5} to 1.15×10^{-2}. Its short persistence limits cumulative direct radiative forcing under the investigated conditions. Together with its reported plasma-processing capability, these findings provide experimental support for CF_3OF as a low-GWP alternative to conventional high-GWP fluorinated process gases.

1. Introduction

The semiconductor and display industries rely on fluorinated gases (F-gases) such as CF_4, C_2F_6, NF_3, and SF_6 for plasma etching and chamber-cleaning processes because these compounds efficiently generate reactive fluorine species under plasma conditions (Song et al., 2022; An and Hong, 2023). During processing, however, a fraction of the supplied gases may remain unreacted, and stable fluorinated by-products may also enter the exhaust stream (Lugani et al., 2024). If not completely destroyed by abatement systems, these compounds can be released into the atmosphere. Many of the long-lived F-gases used in semiconductor and display manufacturing resist the major chemical and photochemical removal processes in the lower atmosphere and consequently persist for centuries to millennia (Ravishankara et al., 1993). Their long atmospheric persistence, combined with strong absorption within the atmospheric infrared window, results in global warming potential (GWP) values several orders of magnitude greater than that of CO_2 (Hodnebrog et al., 2020; Smith et al., 2021). The assessment of an alternative process gas must therefore consider not only process performance but also the

https://doi.org/10.5194/egusphere-2026-6185
Preprint. Discussion started: 16 November 2026
© Author(s) 2026. CC BY 4.0 License.

two principal determinants of its GWP: radiative efficiency (RE) and atmospheric lifetime (Sulbaek Andersen et al., 2017; Hodnebrog et al., 2020).

Against this background, trifluoromethyl hypofluorite (CF_3OF; also denoted CF_4O) is an oxygen-containing F-gas being investigated as a potential alternative process gas for plasma-based semiconductor manufacturing. Recent process studies have shown that CF_3OF-containing mixtures can support selective etching of silicon nitride and have identified COF_2, CF_4, and C_2F_6 among the fluorinated products in the process exhaust (Kim et al., 2025). These observations establish the process relevance of CF_3OF and demonstrate that it participates in plasma chemistry. A nominal 100-year GWP (GWP_{100}) value of approximately 1 has been reported for CF_3OF and has been cited in support of considering it a low-GWP alternative (Kim et al., 2025). However, the basis of this value is not clearly traceable to compound-specific measurements of infrared absorption and atmospheric persistence. Experimental determination of the climate-relevant properties of CF_3OF is therefore required before its GWP can be assessed reliably.

To address this gap, a quantitative assessment of the GWP of CF_3OF requires experimentally grounded values for both its RE and atmospheric lifetime. RE represents the radiative forcing caused by a unit increase in atmospheric abundance and depends on the strength and spectral position of molecular infrared absorption (Pinnock et al., 1995; Shine and Myhre, 2020). The infrared spectroscopic properties of CF_3OF have been examined in a series of earlier studies. Infrared and Raman investigations established its principal vibrational frequencies, relative band intensities, and normal-mode assignments (Lagemann et al., 1952; Wilt and Jones, 1967, 1968; Smardzewski and Fox, 1975). CF_3OF exhibits strong mid-infrared vibrational bands associated principally with C–F stretching, together with C–O and O–F modes. However, these earlier studies focused primarily on band positions, relative intensities, and vibrational assignments and did not provide a molecule-normalized gas-phase absorption cross-section (ACS) spectrum suitable for quantitative RE calculations. Direct Fourier transform infrared (FT-IR) measurements under controlled temperature, pressure, concentration, and optical-path conditions are therefore required.

RE alone, however, is insufficient for a GWP assessment; atmospheric lifetime is the second essential component. CF_3OF is chemically distinct from conventional perfluorocarbons (PFCs), which contain only carbon and fluorine. Its CF_3–O–F framework introduces C–O and O–F bonds in addition to the C–F bonds. The comparatively weak O–F bond is associated with the pronounced oxidizing and fluorinating reactivity of hypofluorites, as demonstrated by reactions with organic substrates and kinetic studies of CF_3OF-initiated oxidation chemistry (Allison and Cady, 1959; dos Santos Afonso and Schumacher, 1984; dos Santos Afonso et al., 2000). Thermal studies showed reversible formation of COF_2 and F_2 and material-dependent decomposition behavior (Porter and Cady, 1957), while mechanistic calculations identified O–F bond activation as a chemically accessible decomposition route (Yin et al., 2002). Because COF_2 is a documented decomposition product of CF_3OF, its subsequent atmospheric behavior is also relevant to the potential removal of CF_3OF-derived carbon. In our previous study, COF_2 underwent rapid conversion under humid, oxygen-containing conditions, accompanied by CO_2 formation (Kim et al., 2026). Taken together, the documented reactivity of CF_3OF and its ability to form COF_2 suggest that its atmospheric persistence may be sensitive to the surrounding gas-phase environment, although the corresponding near-ambient decay timescale has not been established. Time-resolved FT-IR measurements can therefore provide a direct experimental evaluation of CF_3OF decay by monitoring multiple spectrally distinct absorption bands and determining an e-folding decay time from their consistent temporal evolution under controlled conditions.

Accordingly, we apply the general experimental framework previously used by Kim et al. (2026) for COF_2 to quantify the climate-relevant properties of CF_3OF. We determine its gas-phase infrared ACS by quantitative FT-IR spectroscopy and use the measured spectrum to calculate the RE. We then monitor multiple characteristic CF_3OF absorption bands during

https://doi.org/10.5194/egusphere-2026-6185
Preprint. Discussion started: 16 November 2026
© Author(s) 2026. CC BY 4.0 License.

time-resolved experiments in near-anhydrous synthetic air, ambient air spanning a range of absolute humidities, and a 40 % O_2/60 % Ar matrix. The concurrent evolution of the CO_2 absorption band is examined to evaluate its kinetic relationship with CF_3OF loss. The resulting RE and condition-specific e-folding decay times are combined with a lifetime-dependent atmospheric-distribution correction to provide an experimentally based evaluation of the GWP_{100} of CF_3OF.

2. Experimental methods

2.1. Experimental design

The measurements employed the general spectroscopic and time-resolved decay methodology previously reported for COF_2 by Kim et al. (2026), whereas the gas preparation, experimental matrices, spectral analysis, and decay evaluation were adapted specifically for CF_3OF. Because the GWP evaluation requires both RE and atmospheric lifetime, two distinct sets of experiments were conducted. Quantitative infrared spectra were acquired to determine the ACS of CF_3OF and calculate its RE, while time-resolved FT-IR measurements were performed to determine its e-folding decay time under controlled gas-phase conditions.

The decay of CF_3OF was investigated in near-anhydrous synthetic air, ambient air at four absolute humidity levels, and a nitrogen-free matrix containing 40 % O_2 in Ar. These gas matrices were selected to examine the effects of water vapor, oxygen abundance, and bulk gas composition on the observed CF_3OF decay. All decay measurements were performed at a total pressure of 750 ± 1 Torr and a nominal temperature of 298 K. Pressure and temperature were recorded concurrently with each spectrum and monitored throughout each experiment to confirm the physical stability of the sealed measurement system.

2.2. Gas mixtures and preparation

A CF_3OF mixture in N_2, supplied by Sole Materials Co., Ltd. (Republic of Korea), was used as the primary analyte gas. According to the supplier's preparation procedure, CF_3OF was synthesized by reacting COF_2 with F_2 in the presence of CsF, and the product was recovered in a cryogenic collection chamber maintained at approximately −180 °C. The COF_2 precursor was produced by AgF_2-mediated fluorination of CO. The recovered CF_3OF was subsequently prepared gravimetrically as an N_2-based cylinder mixture, with an assigned CF_3OF mole fraction of (908 ± 7) μmol mol^{-1} (k = 2), and was used without further purification.

For the ACS measurements, the parent CF_3OF/N_2 cylinder mixture was first introduced directly into the evacuated FT-IR gas cell to approximately 20.1 Torr. High-purity N_2 was subsequently added until the total pressure reached 80.60 Torr. The CF_3OF mole fraction in the gas cell, calculated from the parent-mixture mole fraction and the measured pressure ratio, was (226 ± 2) μmol mol^{-1} (k = 2). The reported uncertainty includes the propagated contributions from the parent-mixture mole fraction and the pressure measurements made before and after N_2 addition. For the decay experiments, the amount of the CF_3OF/N_2 mixture introduced into the gas cell was adjusted so that the maximum absorbance within the principal CF_3OF absorption region at 1167–1305 cm^{-1} remained below 0.6. This criterion was applied to avoid spectral saturation and maintain the measurements within the linear response range of the FT-IR system.

Near-anhydrous experiments employed synthetic air containing 21 % O_2 in N_2 and approximately 1.6 μmol mol^{-1} H_2O. Ambient outdoor air was introduced through a 2 μm inline particulate filter to provide humid gas matrices. The ambient-air experiments were conducted at absolute water vapor contents of 3.8, 5.2, 19.9, and 22.2 g m^{-3}. A separate nitrogen-free matrix containing 40 % O_2 in Ar was prepared from high-purity O_2 and Ar. N_2 and Ar were treated as chemically inert diluent gases under the experimental conditions; accordingly, comparison of the near-anhydrous 21 % O_2/N_2 and 40 %

https://doi.org/10.5194/egusphere-2026-6185
Preprint. Discussion started: 16 November 2026
© Author(s) 2026. CC BY 4.0 License.

O_2/Ar experiments was used to evaluate the influence of increasing the O_2 mole fraction from 21 % to 40 % on CF_3OF decay.

A certified NF_3/N_2 mixture (299.8 ± 6.0 µmol mol^{-1}; Korea Research Institute of Standards and Science, Republic of Korea) was introduced through a separate gas line. Because NF_3 is chemically stable under the experimental conditions and is present at negligible abundance in ambient air, changes in its infrared signal were used to identify physical gas exchange, including the ingress of ambient air or the loss of gas from the measurement cell.

Before each experiment, the FT-IR gas cell and associated gas-handling lines were evacuated to the 10^{-1} Torr range. For the decay experiments, the CF_3OF/N_2 mixture was first introduced into the evacuated gas cell to a pressure selected according to the absorbance criterion described above. The selected balance gas was subsequently added until the total pressure reached 750 ± 1 Torr. The gases were introduced sequentially and allowed to mix before continuous spectral acquisition was initiated. All pressure-based gas preparations were performed using calibrated capacitance manometers.

Table 1. Compositions, sources, and experimental purposes of the gases used in this study. Reported uncertainties are expanded uncertainties with a coverage factor k = 2, corresponding to an approximately 95 % confidence level.

Gas sample	Composition	Primary use	Supplier or source
CF_3OF / N_2	CF_3OF: 908 ± 7 µmol mol^{-1}	ACS, RE, and decay measurements	Sole Materials Co., Ltd.
NF_3 / N_2	NF_3: 299.8 ± 6.0 µmol mol^{-1}	Indicator of physical gas exchange	Korea Research Institute of Standards and Science
Synthetic air	O_2: 20.9 ± 1.05 % in N_2	CF_3OF decay under near-anhydrous conditions	Union Gas Co., Ltd.
Ambient air	O_2/N_2 atmospheric matrix	CF_3OF decay under humid ambient-air conditions	Collected outdoors
O_2/Ar mixture	40 % O_2 in Ar	CF_3OF decay at elevated O_2 abundance in a nitrogen-free matrix	Union Gas Co., Ltd.

2.3. FT-IR measurements

Infrared measurements were performed using an Arcoptix GASEX OEM FT-IR spectrometer (Arcoptix S.A., Switzerland) coupled to a multipass gas cell with an effective optical path length of 5.00 ± 0.01 m. The spectrometer was equipped with a four-stage thermoelectrically cooled mercury cadmium telluride (4-TEC MCT) detector covering the 833.5–5000 cm^{-1} spectral range. Spectra were acquired at a resolution of 0.5 cm^{-1}, with each spectrum representing the average of 16 scans. The experimental apparatus, including the gas-delivery, FT-IR measurement, and pressure and temperature data-acquisition components, is shown in **Fig. 1**. The FT-IR spectrometer, an MKS 626D Baratron capacitance manometer, a Pt100 platinum resistance temperature detector (RTD), and a Fluke 1586A Super-DAQ precision temperature scanner were integrated into a synchronized measurement system controlled using an in-house LabVIEW program. Temperature and pressure were recorded synchronously with each spectrum to ensure temporal alignment of the spectral and physical measurements.

For the ACS measurements, background and sample intensity spectra were recorded using the same instrumental configuration. For the decay measurements, time-resolved spectral acquisition was initiated after preparation of each experimental gas mixture and continued throughout the experiment. Each measurement cycle consisted of 2.7 s of pressure and temperature acquisition, 10.3 s of FT-IR spectral acquisition, and a 47 s idle period, producing synchronized pressure, temperature, and spectral datasets at one-minute intervals.

https://doi.org/10.5194/egusphere-2026-6185
Preprint. Discussion started: 16 November 2026
© Author(s) 2026. CC BY 4.0 License.

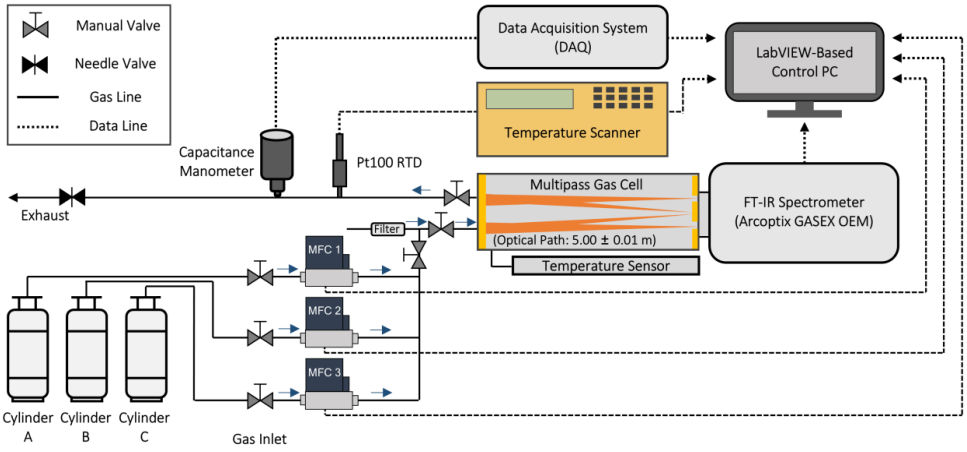


Figure 1. Schematic of the experimental apparatus used to determine the ACS and measure the time-resolved decay of CF_3OF. The system comprised three gas cylinders (A, a CF_3OF/N_2 mixture; B, synthetic air or an O_2/Ar mixture; and C, an NF_3/N_2 mixture), each connected to an independently controlled mass flow controller (MFC); a multipass gas cell with an effective optical path length of 5.00 ± 0.01 m; and an Arcoptix GASEX OEM FT-IR spectrometer. The pressure and temperature inside the gas cell were measured using a capacitance manometer and an inline Pt100 RTD, respectively. The RTD was connected to a temperature scanner. For experiments using ambient air, outdoor air was introduced through a filtered intake line. FT-IR spectral acquisition and synchronous pressure and temperature logging were managed using a LabVIEW-based control and data acquisition system.

2.4. Determination of ACS and RE

The spectral transmittance ($Tr(\tilde{\nu})$) and absorbance ($A(\tilde{\nu})$) at wavenumber $\tilde{\nu}$ were calculated from the measured background and sample intensities as:

$$Tr(\tilde{\nu}) = I(\tilde{\nu})/I_0(\tilde{\nu}) \quad (1)$$

$$A(\tilde{\nu}) = -\log[Tr(\tilde{\nu})] = -\log[I(\tilde{\nu})/I_0(\tilde{\nu})] \quad (2)$$

where $I_0(\tilde{\nu})$ and $I(\tilde{\nu})$ are the background and sample intensities, respectively. Transmittance was used to calculate the ACS, whereas absorbance was used for the band-integration analysis of the time-resolved decay measurements described in Sect. 2.5.

The ACS of CF_3OF was calculated from the measured transmittance using the Beer–Lambert law combined with the ideal gas law (Harrison, 2020):

$$\sigma(\tilde{\nu}) = \frac{\ln(1/T_r(\tilde{\nu})) \cdot \mathrm{R} \cdot T}{P_{Total} \cdot x_{CF3OF} \cdot 10^{-6} \cdot L \cdot N_A} \quad (3)$$

where $\sigma(\tilde{\nu})$ is the ACS at wavenumber $\tilde{\nu}$ (cm^2 molecule^{-1}), R is the gas constant (6.23637 × 10^4 cm^3 Torr mol^{-1} K^{-1}), T is the measured gas temperature (K), P is the total pressure (Torr), x_{CF3OF} is the numerical value of the CF_3OF mole fraction expressed in µmol mol^{-1}, L is the effective optical path length (cm), and N_A is the Avogadro constant (6.0221 × 10^{23} molecule mol^{-1}). Thus, $P \cdot x_{CF3OF} \cdot 10^{-6}$ is the partial pressure of CF_3OF in Torr.

For the RE calculation, following the absorption-spectrum-based approach of Pinnock et al. (1995), the measured ACS spectrum was averaged onto the 10 cm^{-1} wavenumber grid of the stratospheric-adjusted Pinnock curve developed by Shine and Myhre (2020). This curve provides the radiative forcing per unit ACS as a function of wavenumber. The ACS assigned to each grid point was calculated as the arithmetic mean of all measured ACS values within the corresponding 10 cm^{-1} interval; for example, the value assigned at 845 cm^{-1} was the mean over $840 \le \tilde{\nu} < 850$ cm^{-1}. At each grid point, the mean

https://doi.org/10.5194/egusphere-2026-6185
Preprint. Discussion started: 16 November 2026
© Author(s) 2026. CC BY 4.0 License.

ACS was multiplied by the corresponding value of the stratospheric-adjusted Pinnock curve, and the resulting products were integrated over the measured infrared spectral range:

$$\mathrm{RE} = \sum_i \sigma_i F_i \Delta\tilde{\nu} \quad (4)$$

where σ_i is the mean ACS in grid interval i, F_i is the corresponding value of the stratospheric-adjusted Pinnock curve, and $\Delta\tilde{\nu}$ = 10 cm^{-1}. This calculation yielded the RE on a mixing-ratio basis (W m^{-2} ppb^{-1}).

2.5. Experimental evaluation of atmospheric lifetime

The atmospheric lifetime of CF_3OF was evaluated experimentally from its *e*-folding decay time in background gas matrices differing in composition and water-vapor content. The temporal change in CF_3OF was quantified from the integrated absorbance of its characteristic composite absorption band over 1167–1305 cm^{-1}. For each gas matrix, the non-normalized integrated absorbance was fitted using a single-exponential decay function:

$$S(t) = S_\infty + A\,exp(-\frac{t}{\tau}) \quad (5)$$

where $S(t)$ is the integrated CF_3OF absorbance at elapsed time t, S_∞ is the fitted asymptotic signal, A is the fitted decay amplitude, and τ is the *e*-folding decay time. Time was referenced to the beginning of the fitted interval, such that t = 0 represents the first data point included in the fit. The corresponding apparent first-order decay constant is $k_{app} = 1/\tau$. Within this single-exponential framework, the fitted τ for each gas matrix was taken as the experimentally evaluated, condition-specific atmospheric lifetime of CF_3OF and was used in the subsequent calculations of absolute global warming potential (AGWP) and GWP over a 100-year time horizon.

To compare the CF_3OF decay profiles independently of differences in initial signal magnitude and residual absorbance, each dataset was subsequently normalized using its individually fitted amplitude and asymptotic signal as $S_{norm}(t) = [S(t) - S_\infty]/A = [S(t) - S_\infty]/[S(0) - S_\infty]$. Because $S(0) = S_\infty + A$, the corresponding normalized fitted function is $S_{fit,norm}(t) = \exp(-t/\tau)$. This transformation sets the fitted signal at t = 0 and its asymptotic value to 1 and 0, respectively, allowing the shapes of the decay curves to be compared directly. At $t = \tau$, the normalized fitted signal decreases to $1/e$ of its initial value. Because normalization was applied only after fitting the non-normalized integrated absorbance data, it did not alter the fitted value of τ. The resulting τ values were used to compare CF_3OF persistence among the near-anhydrous synthetic-air, humid ambient-air, and O_2/Ar matrices.

2.6. GWP_{100} calculation

The 100-year GWP of CF_3OF was evaluated using the AGWP framework adopted in contemporary climate assessments (Hodnebrog et al., 2013, 2020; Myhre et al., 2013; Smith et al., 2021). GWP is defined as the ratio of the time-integrated radiative forcing resulting from a 1 kg pulse emission of gas i at t = 0 to that resulting from an equivalent 1 kg pulse emission of CO_2 over a selected time horizon H:

$$GWP_i(\mathrm{H}) = \frac{AGWP_i(H)}{AGWP_{CO2}(H)} = \frac{\int_0^H RF_i(\mathrm{t})dt}{AGWP_{CO2}(H)} \quad (6)$$

For a non-CO_2 gas with a single dominant atmospheric sink, the atmospheric burden following a pulse emission decreases exponentially, and the corresponding AGWP is expressed as:

$$AGWP_i(H) = \int_0^H RF_i(\mathrm{t})dt = \int_0^H RE_{i,mass} \cdot \exp(-\frac{t}{\tau_i})\,dt \quad (7)$$

https://doi.org/10.5194/egusphere-2026-6185
Preprint. Discussion started: 16 November 2026
© Author(s) 2026. CC BY 4.0 License.

Evaluation of the integral in Eq. (7) gives $RE_{i,mass}\ \tau_i\ [1\ -\ \exp(-\frac{H}{\tau_i})]$, where $RE_{i,mass}$ (W m^{-2} kg^{-1}) is the mass-based RE of gas i, τ_i (years) is its experimentally determined e-folding decay time, and H = 100 years is the time horizon used in this study. The term $\tau_i\ [1\ -\ \exp(-\frac{H}{\tau_i})]$ is the integrated lifetime factor and accounts for temporal decay of the atmospheric burden over the selected time horizon. The lifetime-dependent correction for the restricted atmospheric distribution of CF_3OF was then applied through Eq. (8).

The mixing-ratio-based RE was converted to a mass basis as $RE_{i,mass} = RE_{i,ppb} \times (M_{air}/M_i) \times (10^9/m_{atm})$ (Hodnebrog et al., 2013). Here, M_{air} = 28.97 g mol^{-1} is the mean molar mass of dry air, M_i = 104.00 g mol^{-1} is the molar mass of CF_3OF, and m_{atm} = 5.1352 × 10^{18} kg is the mean dry mass of the atmosphere (Trenberth and Smith, 2005). Experimentally determined decay times were converted from minutes to years using 1 yr = 365 days. The reference $AGWP_{CO2}(100)$ used in Eq. (6) was 8.95 × 10^{-14} W m^{-2} yr kg^{-1} (Smith et al., 2021).

Because rapid near-surface removal may prevent CF_3OF from attaining the globally uniform distribution assumed in the Pinnock-curve RE calculation, a lifetime-dependent fractional factor was evaluated using the hydroxyl radical (OH)-type parameterization of Hodnebrog et al. (2013, 2020):

$$\mathrm{f}(\tau) = \frac{a\tau^b}{1 + c\tau^d}, \qquad (8)$$

where a = 2.962, b = 0.9312, c = 2.994, d = 0.9302, and τ is expressed in years. The parameterization is defined over $10^{-4} < \tau < 10^4$ years and approaches zero for very short-lived species and unity for long-lived, well-mixed species. The parameterization was developed for compounds removed predominantly by tropospheric OH. This lifetime-dependent parameterization was used to account for the restricted atmospheric distribution of short-lived CF_3OF. The final AGWP used in this study was therefore calculated as:

$$AGWP_i(H)\ =\ f(\tau_i)\ RE_{i,mass}\ \tau_i\ [1\ -\ \exp(-\frac{H}{\tau_i})] \qquad (9)$$

The corresponding $GWP_i(H)$ was obtained by dividing $AGWP_i(H)$ by the reference AGWP of CO_2 over the same time horizon, according to Eq. (6). Thus, $f(\tau_i)$ corrects the RE for restricted atmospheric distribution, whereas $\tau_i\ [1\ -\ \exp(-\frac{H}{\tau_i})]$ accounts for integration of the decaying atmospheric burden over the selected time horizon. The $AGWP_{100}$ and GWP_{100} values reported as the principal climate metrics in this study were calculated using Eq. (9).

3. Results and discussion

3.1. Infrared absorption spectrum and ACS

The gas-phase infrared ACS spectrum of CF_3OF measured in this study is shown in **Fig. 2**. The spectrum was obtained at 296.74 K and a total pressure of 80.60 Torr using a CF_3OF mole fraction of 226 μmol mol^{-1}, an effective optical path length of 500 cm, and a spectral resolution of 0.5 cm^{-1}. It was dominated by an intense, structured absorption band within the selected interval of 1167–1305 cm^{-1}, with a maximum ACS of approximately 3.0 × 10^{-18} cm^2 molecule^{-1} at 1262.50 cm^{-1}. Four band maxima were identified at 947.50, 1222.75, 1262.50, and 1294.25 cm^{-1}. Overall, the quantitatively significant absorption of CF_3OF was concentrated predominantly within the 1167–1305 cm^{-1} region, and no substantial absorption attributable to CF_3OF was observed above 3000 cm^{-1}. The corresponding pointwise ACS uncertainty budget is provided in **Table S1** of the Supplementary Information (SI).

https://doi.org/10.5194/egusphere-2026-6185
Preprint. Discussion started: 16 November 2026
© Author(s) 2026. CC BY 4.0 License.

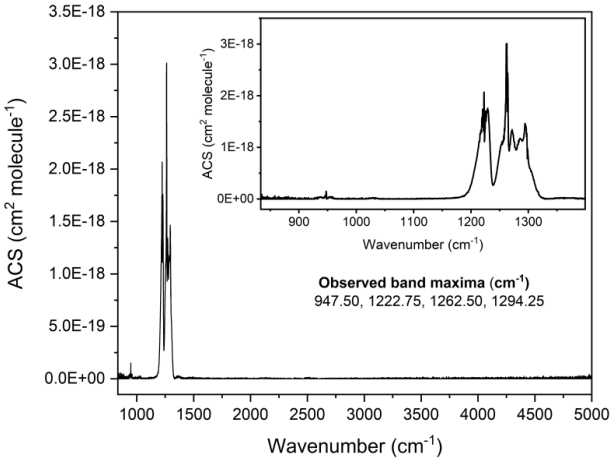


Figure 2. Gas-phase infrared ACS spectrum of CF_3OF measured at 296.74 K and a total pressure of 80.60 Torr using a CF_3OF mole fraction of 226 µmol mol^{-1}, an effective optical path length of 500 cm, and a spectral resolution of 0.5 cm^{-1}. The inset provides an expanded view of the principal absorption region. The observed maxima at 947.50, 1222.75, 1262.50, and 1294.25 cm^{-1} correspond predominantly to the C–O stretching mode and three CF_3 stretching fundamentals, respectively.

The observed maxima agree closely with the gas-phase infrared bands reported at 947.3, 1223.2, 1262.5, and 1294.4 cm^{-1} in **Table 1** of Wilt and Jones (1967), differing by no more than 0.45 cm^{-1}. The maxima at 1222.75, 1262.50, and 1294.25 cm^{-1} are assigned to the principal C–F stretching modes of CF_3OF reported in previous vibrational studies (Lagemann et al., 1952; Aymonino, 1965; Wilt and Jones, 1968). Their close spacing and strong intensities account for the complex structure of the dominant absorption envelope. The maximum at 947.50 cm^{-1} is attributed predominantly to C–O stretching, consistent with the later spectroscopic assignment of Smardzewski and Fox (1975). The expected O–F stretching feature near 883 cm^{-1} was considerably weaker and was not resolved as a distinct maximum in the present spectrum.

Previous spectroscopic studies established the vibrational frequencies, relative intensities, band contours, and mode assignments of CF_3OF (Lagemann et al., 1952; Aymonino, 1965; Wilt and Jones, 1967, 1968; Smardzewski and Fox, 1975), but did not provide molecule-normalized ACS suitable for RE calculations. To the best of our knowledge, quantitative gas-phase infrared ACS data for CF_3OF over the 833.5–5000 cm^{-1} range have not previously been reported. The present measurements address this gap by extending the earlier frequency-based spectroscopic characterization of CF_3OF to a quantitative ACS scale expressed in cm^2 $molecule^{-1}$. The measured ACS over 833.5–3000 cm^{-1}, corresponding to the experimentally covered portion of the 0–3000 cm^{-1} spectral domain of the Pinnock curve, was integrated to yield 1.25×10^{-16} cm $molecule^{-1}$. This result provides the quantitative spectral basis for calculating the RE of CF_3OF.

3.2. RE

Figure 3 summarizes the conversion of the measured CF_3OF ACS into RE. As described in Sect. 2.4, the ACS spectrum was averaged onto the 10 cm^{-1} grid of the stratospheric-adjusted Pinnock curve reported by Shine and Myhre (2020), which was used as the spectral weighting function in the RE calculation according to Eq. (4). **Figure 3a** compares the resulting ACS spectrum with this weighting curve. The most pronounced overlap occurs within the gray-shaded region at approximately 1167–1305 cm^{-1}, where the intense CF_3OF absorption envelope associated predominantly with C–F stretching coincides with relatively large Pinnock-curve values. The weaker CF_3OF absorption feature in the 925–975 cm^{-1}

https://doi.org/10.5194/egusphere-2026-6185
Preprint. Discussion started: 16 November 2026
© Author(s) 2026. CC BY 4.0 License.

region also overlaps with a radiatively effective spectral region but makes a substantially smaller contribution because of its lower cross-section.

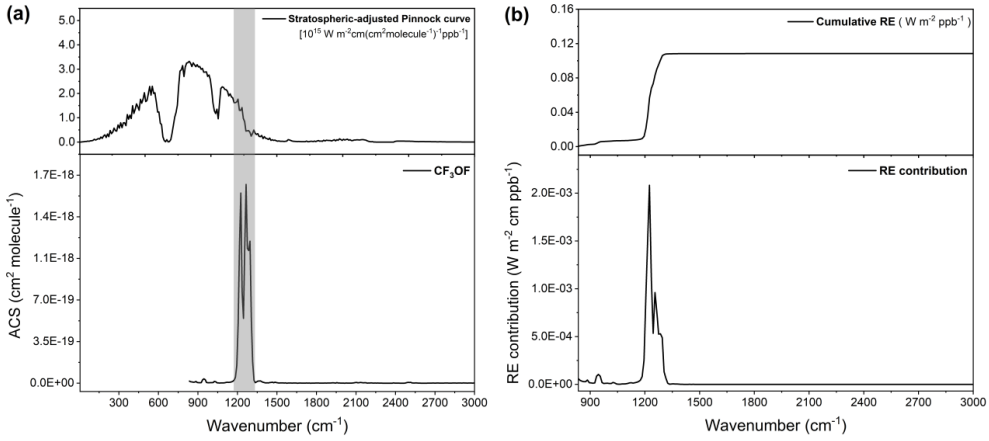


Figure 3. Determination of the mixing-ratio-based RE of CF_3OF from its measured infrared ACS and the stratospheric-adjusted Pinnock curve. Before the RE calculation, the measured ACS spectrum was averaged onto the 10 cm^{-1} wavenumber grid of the Pinnock curve. **(a)** The upper panel shows the stratospheric-adjusted Pinnock curve reported by Shine and Myhre (2020), and the lower panel shows the corresponding 10 cm^{-1}-averaged ACS spectrum of CF_3OF. The gray-shaded region at approximately 1167–1305 cm^{-1} highlights the coincidence of the principal CF_3OF absorption envelope with the descending high-wavenumber wing of the Pinnock curve. Consequently, the lower-wavenumber portion of this absorption envelope receives greater radiative weighting than its higher-wavenumber portion. **(b)** The lower panel shows the spectral RE contribution calculated at each grid point as the product of the CF_3OF ACS and the corresponding Pinnock-curve value according to Eq. (4). The upper panel shows the cumulative integral of the spectral RE contribution over wavenumber. The pronounced increase across the main absorption band, followed by a plateau near 1365 cm^{-1}, reflects the dominant contribution of this band to the resulting mixing-ratio-based RE of 0.108 W m^{-2} ppb^{-1}.

Pointwise multiplication of the ACS and Pinnock-curve values produced the RE-contribution spectrum shown in the lower panel of **Fig. 3b**. The spectrum is dominated by the structured contribution within 1167–1305 cm^{-1}, whereas only minor contributions occur below 1000 cm^{-1}. Across the principal CF_3OF absorption envelope highlighted in **Fig. 3a**, the Pinnock-curve value decreases with increasing wavenumber. Consequently, the lower-wavenumber portion of the CF_3OF band receives greater radiative weighting, whereas its higher-wavenumber features are progressively suppressed. This spectral weighting produces the asymmetric RE-contribution profile shown in **Fig. 3b** and shifts the strongest contribution toward the lower-wavenumber portion of the absorption envelope rather than the position of the maximum ACS at 1262.50 cm^{-1}. Although the principal CF_3OF band overlaps a radiatively effective spectral region, much of the band lies along the descending high-wavenumber wing of the Pinnock curve. Its radiative contribution is therefore moderated relative to that expected if the same absorption strength coincided with the region of maximum Pinnock-curve weighting. Consistent with this distribution, the cumulative RE increases gradually at lower wavenumbers and then rises sharply across the principal CF_3OF absorption envelope, reaching essentially its final value by approximately 1365 cm^{-1}. The cumulative curve remains nearly constant thereafter, indicating little additional contribution from the higher-wavenumber portion of the measured spectrum.

The integrated ACS of CF_3OF over 833.5–3000 cm^{-1} was 1.25×10^{-16} cm $molecule^{-1}$, and integration of the corresponding RE-contribution spectrum yielded a mixing-ratio-based RE of 0.108 W m^{-2} ppb^{-1}. Despite the moderating effect of its spectral position on the Pinnock-curve weighting, this RE indicates that CF_3OF has appreciable radiative strength per unit atmospheric abundance. However, this value represents the RE calculated for a globally and uniformly distributed gas

https://doi.org/10.5194/egusphere-2026-6185
Preprint. Discussion started: 16 November 2026
© Author(s) 2026. CC BY 4.0 License.

before accounting for the restricted atmospheric distribution expected for a short-lived compound; therefore, it does not by itself determine the GWP of CF_3OF. Its cumulative climate impact consequently depends strongly on its atmospheric lifetime and the corresponding lifetime-dependent distribution correction, as evaluated in the following sections (Hodnebrog et al., 2013, 2020).

3.3. Time-resolved CF_3OF decay, CO_2 formation, and proposed conversion pathway

Time-resolved FT-IR spectra acquired in near-anhydrous synthetic air containing 21 % O_2 in N_2 showed simultaneous but opposing changes in the CF_3OF and CO_2 absorption bands in **Fig. 4a**. The characteristic CF_3OF absorption envelope within 1167–1305 cm^{-1} decreased progressively while retaining its overall spectral shape, whereas the CO_2 asymmetric-stretching band within the 2284–2391 cm^{-1} integration range increased above its initial background level. The NF_3 tracer band remained essentially unchanged throughout the experiment, indicating negligible physical gas exchange with the surroundings. These spectral changes therefore indicate that CF_3OF was removed within the gas cell while CO_2 accumulated concurrently.

The integrated CF_3OF absorbance over 1167–1305 cm^{-1} was fitted using $S(t) = C + A \cdot exp(-t/\tau)$, yielding an e-folding decay time of 3451 min (57.5 h; **Fig. 4b** and **Table 2**). The integrated CO_2 absorbance over 2284–2391 cm^{-1} was fitted using the equivalent rise function, $S(t) = C - A \cdot exp(-t/\tau)$, and yielded a characteristic rise time of 3591 min (59.8 h; **Fig. 4c** and **Table 2**). Both temporal profiles were well described by the single-exponential functions ($R^2 > 0.997$), supporting comparison of their characteristic times. The two characteristic times differed by only 4.1 %. This close agreement, together with the opposing temporal evolution of the independently monitored signals, indicates that CF_3OF loss and CO_2 formation were kinetically associated under the investigated conditions. The fitting parameters and coefficients of determination are reported in **Table S2** of the SI.

The close correspondence between CF_3OF decay and CO_2 formation supports the conversion of CF_3OF-derived carbon to CO_2 on approximately the same characteristic timescale. CF_3OF may undergo oxidative conversion to CO_2 through a COF_2-independent pathway, either directly or through other short-lived intermediates. Alternatively, CF_3OF may first form COF_2, which is subsequently converted to CO_2. The latter pathway is chemically plausible because previous studies identified COF_2 as an accessible product of CF_3OF decomposition (Porter and Cady, 1957), while theoretical and experimental investigations have shown that COF_2 can be converted to CO_2 under water-containing conditions (Francisco, 1993; Zachariah et al., 1995; Uchimaru et al., 2004; Kim et al., 2026).

No spectral features attributable to COF_2 or other intermediates were observed during CF_3OF decay. With spectra acquired at one-minute intervals, a rapidly formed and consumed intermediate or a low steady-state COF_2 abundance would not necessarily be resolved. Taken together, the coupled CF_3OF and CO_2 kinetics and the absence of detectable intermediate signals suggest that the overall conversion proceeded without detectable accumulation of persistent carbon-containing intermediates. Whether this behavior reflects a COF_2-independent pathway or rapid turnover of transient COF_2 remains an important mechanistic question for investigations employing higher temporal resolution and greater sensitivity to potential intermediates.

https://doi.org/10.5194/egusphere-2026-6185
Preprint. Discussion started: 16 November 2026
© Author(s) 2026. CC BY 4.0 License.

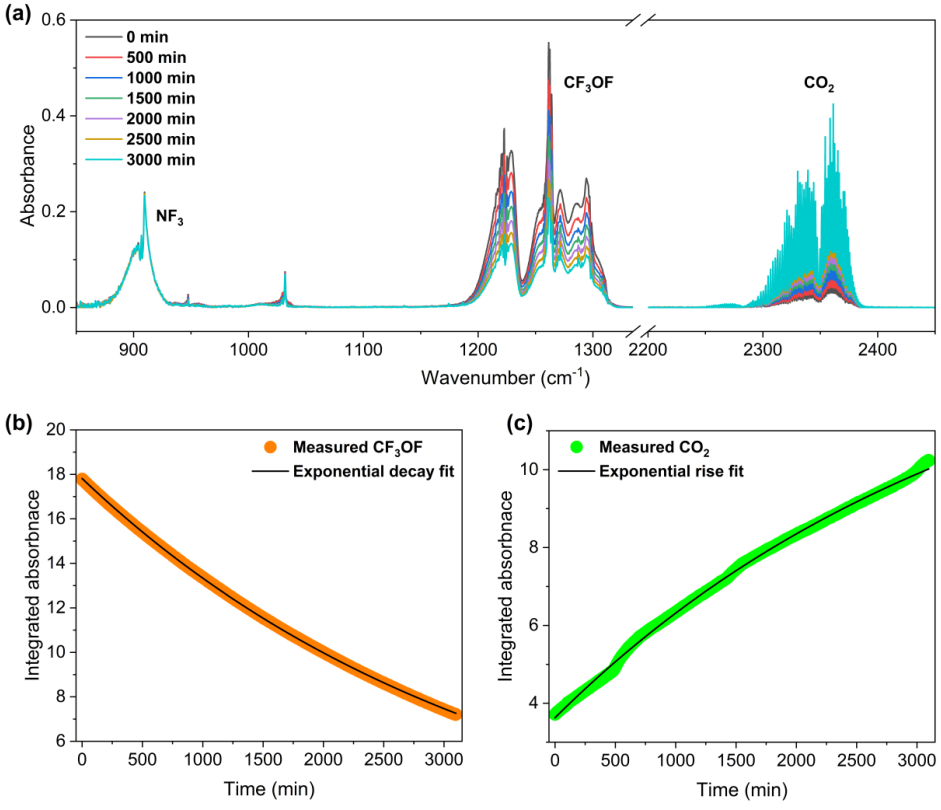


Figure 4. Time-resolved FT-IR observation of CF_3OF decay and CO_2 formation in near-anhydrous synthetic air containing 21 % O_2 in N_2. **(a)** Selected absorbance spectra showing the progressive decrease in the CF_3OF absorption bands within 1167–1305 cm^{-1} and the concurrent increase in the CO_2 absorption band within 2284–2391 cm^{-1}, while the NF_3 tracer band within 867–935 cm^{-1} remained essentially unchanged throughout the experiment. Spectra were acquired at 1 min intervals, and representative spectra are displayed at 500 min intervals. **(b)** Integrated CF3OF absorbance over 1167–1305 cm^{-1} and the corresponding single-exponential decay fit. **(c)** Integrated CO_2 absorbance over 2284–2391 cm^{-1} and the corresponding single-exponential rise fit.

3.4. Effects of humidity and gas composition on CF_3OF decay

To determine how gas-phase water vapor affects the persistence of CF_3OF, time-resolved decay experiments were conducted using outdoor ambient air containing 3.8, 5.2, 19.9, and 22.2 g m^{-3} H_2O. **Figure 5** compares the spectral and kinetic behavior observed at 3.8 and 19.9 g m^{-3} H_2O, which were selected as representative lower- and higher-humidity ambient-air conditions, respectively. At 3.8 g m^{-3} H_2O, the CF_3OF absorption envelope within 1167–1305 cm^{-1} decreased gradually throughout the 3100 min observation period, with an e-folding decay time of 2448 min (**Fig. 5a** and **b**; **Table 2**). At 19.9 g m^{-3} H_2O, the measured integrated CF_3OF absorbance fell below 10 % of its initial value by 530 min, with an e-folding decay time of 203 min (**Fig. 5c** and **d**; **Table 2**). Thus, increasing the absolute humidity from 3.8 to 19.9 g m^{-3} shortened the CF_3OF decay time by a factor of approximately 12.0. The NF_3 tracer band remained essentially unchanged in both experiments, confirming that the pronounced difference in CF_3OF decay was not caused by leakage, dilution, or physical gas exchange with the surroundings.

https://doi.org/10.5194/egusphere-2026-6185
Preprint. Discussion started: 16 November 2026
© Author(s) 2026. CC BY 4.0 License.

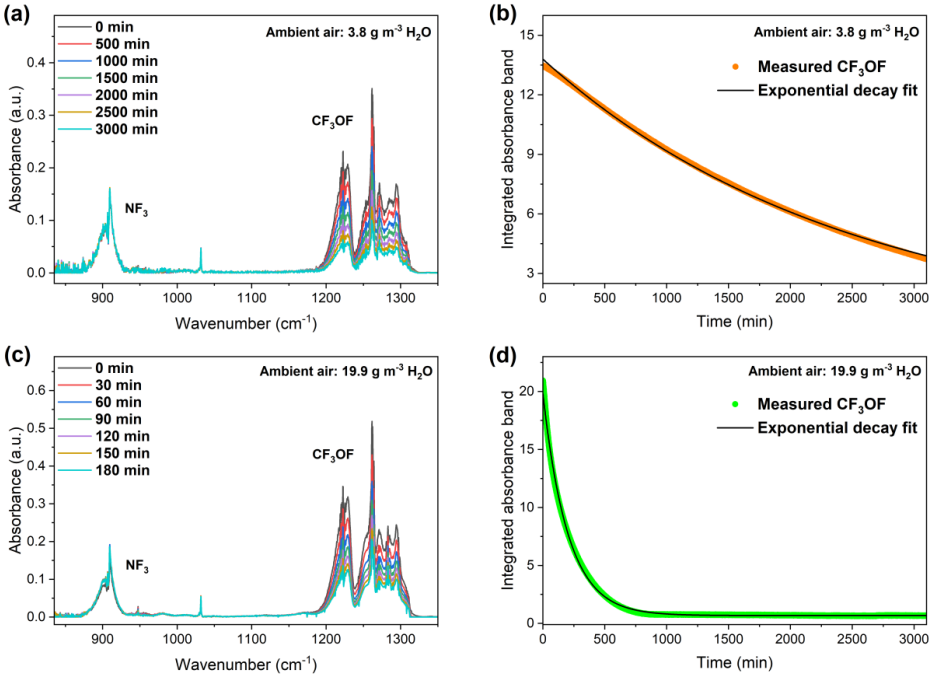


Figure 5. Effect of absolute humidity on the time-resolved decay of CF_3OF in ambient air. **(a)** and **(b)** FT-IR spectra and integrated CF_3OF absorbance measured at an absolute humidity of 3.8 g m^{-3}. **(c)** and **(d)** Corresponding measurements at an absolute humidity of 19.9 g m^{-3}. Panels **(a)** and **(c)** show the progressive decrease in the CF_3OF absorption bands within 1167–1305 cm^{-1}, while the NF_3 tracer band within 867–935 cm^{-1} remained essentially unchanged. Representative spectra are displayed at 500 min intervals in panel **(a)** and at 30 min intervals in panel **(c)** to resolve the different decay timescales. Panels **(b)** and **(d)** show the integrated CF_3OF absorbance over 1167–1305 cm^{-1} and the corresponding single-exponential decay fits.

The six CF_3OF decay profiles are compared on a common normalized scale in **Fig. 6a**. Normalization places all decay profiles on a common scale from 1 to 0 without changing the fitted e-folding decay time, thereby allowing their relative decay rates to be compared directly. The τ values were obtained by fitting the non-normalized measurements. The near-anhydrous synthetic-air experiment exhibited the slowest decay, with τ = 3451 min. In ambient air, τ decreased successively to 2448 and 1974 min at 3.8 and 5.2 g m^{-3} H_2O and then to 203 and 168 min at 19.9 and 22.2 g m^{-3} H_2O, respectively (**Table 2** and **Fig. 6b**). Relative to the near-anhydrous reference condition, the two highest-humidity conditions shortened the decay time by factors of 17.0 and 20.5.

The humidity-dependent decrease in τ was markedly non-uniform over the investigated range. The decrease was moderate between the near-anhydrous reference and the two lower-humidity ambient-air conditions but exceeded an order of magnitude at 19.9 and 22.2 g m^{-3} H_2O. This behavior demonstrates that water vapor strongly promotes CF_3OF removal under the applied gas-phase conditions. The humidity response is consistent with water participating in, or facilitating, one or more stages of CF_3OF transformation, including its initial loss, subsequent conversion of short-lived products, or both. Although the present measurements do not resolve the individual elementary steps, they establish absolute humidity as a major experimental variable controlling the persistence of CF_3OF.

The effect of O_2 abundance was examined by comparing the two near-anhydrous gas matrices in **Fig. 6c**. The e-folding decay time decreased from 3451 min in synthetic air containing 21 % O_2 in N_2 to 2704 min in the 40 % O_2/60 % Ar matrix,

https://doi.org/10.5194/egusphere-2026-6185
Preprint. Discussion started: 16 November 2026
© Author(s) 2026. CC BY 4.0 License.

corresponding to a reduction of approximately 22 %. Because N_2 and Ar served as inert balance gases and the water-vapor content was negligible in both experiments, this result demonstrates that increasing the O_2 mole fraction accelerated CF_3OF removal under the applied conditions. The observed dependence on O_2 abundance indicates that oxygen participates in, or facilitates, the overall CF_3OF removal process. However, measurements at only two O_2 mole fractions are insufficient to establish the reaction order with respect to O_2 or to identify the specific oxygen-dependent reaction step.

The CO_2 response in the 40 % O_2/60 % Ar matrix provides additional information about the relationship between CF_3OF removal and subsequent carbon-containing products in **Fig. 6d**. The integrated CO_2 absorbance over 2284–2391 cm^{-1} increased overall during CF_3OF decay, demonstrating that CO_2 formation also occurred in the oxygen-enriched matrix. However, unlike the CO_2 response in near-anhydrous synthetic air, the temporal increase was not adequately represented by a single-exponential rise and was therefore not assigned a characteristic rise time. Although CF_3OF decayed more rapidly in the oxygen-enriched matrix, its faster disappearance was not accompanied by a correspondingly simple acceleration of CO_2 accumulation. This difference indicates that increased CF_3OF removal does not translate directly into an immediate one-step formation of CO_2. Instead, the observed behavior is consistent with additional transformation steps, transient intermediates, or parallel reaction pathways between the initial loss of CF_3OF and the eventual accumulation of CO_2.

Overall, CF_3OF decay was sensitive to both absolute humidity and gas composition. Among the conditions investigated, the acceleration observed in high-humidity ambient air was substantially greater than the difference between the two near-anhydrous matrices. Water vapor therefore exerted the strongest observed influence on CF_3OF persistence, while the oxygen-enriched O_2/Ar experiment showed that the surrounding gas matrix can additionally affect both CF_3OF removal and the temporal behavior of CO_2 formation. The resulting condition-specific e-folding decay times provide the experimental basis for the atmospheric-lifetime and GWP_{100} evaluations presented in Sect. 3.6.

Table 2. Condition-dependent characteristic times (τ) for CF_3OF decay and CO_2 formation under the investigated gas matrices. Values are rounded to the nearest minute. The fitting parameters, coefficients of determination and standard errors are provided in **Table S2** of the SI; fitting precision is summarized in Sect. 3.5.

Gas matrix	Humidity condition	Kinetic process	τ (min)
Synthetic air (21 % O_2/N_2)	Near-anhydrous	CF_3OF decay	3451
	Near-anhydrous	CO_2 formation	3591
40 % O_2/60 % Ar	Near-anhydrous	CF_3OF decay	2704
Ambient air	3.8 g m^{-3} H_2O	CF_3OF decay	2448
Ambient air	5.2 g m^{-3} H_2O	CF_3OF decay	1974
Ambient air	19.9 g m^{-3} H_2O	CF_3OF decay	203
Ambient air	22.2 g m^{-3} H_2O	CF_3OF decay	168

https://doi.org/10.5194/egusphere-2026-6185
Preprint. Discussion started: 16 November 2026
© Author(s) 2026. CC BY 4.0 License.

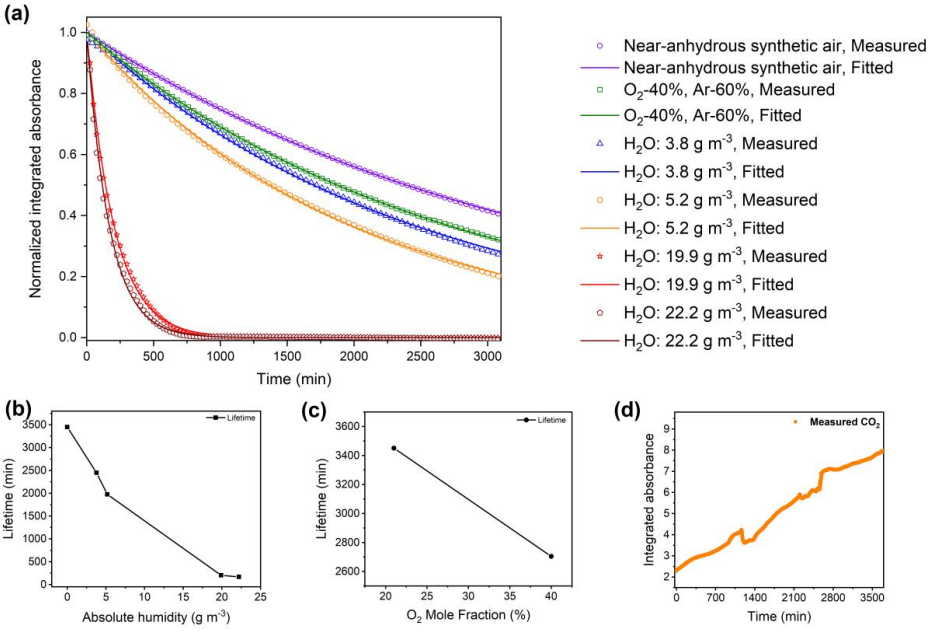


Figure 6. Comparison of normalized CF_3OF decay profiles, derived e-folding decay times, and CO_2 formation under different gas-phase conditions. **(a)** Normalized integrated CF_3OF absorbance over 1167–1305 cm^{-1} as a function of elapsed time in near-anhydrous synthetic air, a 40 % O_2/60 % Ar matrix, and ambient air containing 3.8–22.2 g m^{-3} H_2O. Symbols represent measured values, and solid lines represent the corresponding single-exponential fits. **(b)** CF_3OF e-folding decay time, τ, as a function of absolute humidity in near-anhydrous synthetic air and ambient air. The near-anhydrous synthetic-air condition is represented as 0 g m^{-3} H_2O on the displayed scale. **(c)** Comparison of the CF_3OF e-folding decay times obtained under near-anhydrous conditions in synthetic air containing 21 % O_2 in N_2 and in the 40 % O_2/60 % Ar matrix. **(d)** Time-dependent integrated CO_2 absorbance over 2284–2391 cm^{-1} in the 40 % O_2/60 % Ar matrix, showing the overall accumulation of CO_2 during CF_3OF decay.

3.5. Uncertainties

At the principal ACS maximum (1262.50 cm^{-1}), an approximate budget combining the evaluated mole-fraction, temperature, pressure, path-length and transmittance contributions yielded a combined relative standard uncertainty of 0.49 % and an expanded relative uncertainty of 0.97 % (k = 2). The transmittance standard uncertainty, 6.02×10^{-4}, was estimated from the standard deviation of the processed spectrum in the non-absorbing 2700–3000 cm^{-1} region. **Table S1** of the SI gives the input values, their sources adopted assumptions and propagation equation for this pointwise assessment. The relative standard errors of the fitted CF_3OF decay times were 0.02–0.25 %; the corresponding value for CO_2 formation in near-anhydrous synthetic air was 0.59 % (**Table S2** of the SI). These values describe the statistical precision of the fitted characteristic times. The atmospheric interpretation of the decay times and GWP_{100} estimates is discussed in Sect. 3.6.

3.6. Experimentally constrained atmospheric persistence and GWP_{100}

The experimentally determined e-folding decay times ranged from 3.20×10^{-4} to 6.57×10^{-3} years, equivalent to approximately 2.8–57.5 h, across the investigated gas matrices (**Table 3**). These short persistence times were obtained under controlled near-surface conditions containing atmospheric constituents relevant to CF_3OF removal, including O_2 and varying amounts of water vapor. If the observed behavior is representative of that in the lower atmosphere, CF_3OF would be removed well before becoming globally mixed or undergoing appreciable transport to the stratosphere. Its atmospheric

https://doi.org/10.5194/egusphere-2026-6185
Preprint. Discussion started: 16 November 2026
© Author(s) 2026. CC BY 4.0 License.

persistence would therefore be governed primarily by removal processes operating in the troposphere rather than by stratospheric photolysis.

The strong dependence of the measured decay time on absolute humidity further indicates that CF_3OF persistence may vary with regional and seasonal atmospheric conditions. Shorter decay times would be expected in warm or humid environments, whereas comparatively longer persistence may occur under dry conditions. The observed sensitivity to O_2 abundance also supports the involvement of the oxygen-containing gas matrix in the overall removal process. These experiments do not reproduce all atmospheric transport, photochemical, and heterogeneous processes; nevertheless, they provide direct experimental constraints on the persistence of CF_3OF in atmospherically relevant near-surface gas matrices. Reaction with OH in the troposphere may provide an additional atmospheric sink, but its contribution cannot be quantified without a compound-specific reaction rate coefficient (Kurylo and Orkin, 2003) and was therefore not explicitly included in the present lifetime evaluation.

The mixing-ratio-based RE of 0.108 W m^{-2} ppb^{-1} corresponds to a mass-based RE of 5.86×10^{-12} W m^{-2} kg^{-1}. The lifetime-dependent distribution factor, $f(\tau)$, decreased from 0.02674 in near-anhydrous synthetic air to 0.00164 in ambient air containing 22.2 g m^{-3} H_2O. Applying this factor to the mass-based RE yielded distribution-adjusted RE values ranging from 1.57×10^{-13} to 9.63×10^{-15} W m^{-2} kg^{-1}. This correction represents the increasingly restricted atmospheric distribution expected as the lifetime of CF_3OF becomes shorter. Use of these values in Eq. (9) yielded $AGWP_{100}$ values of 1.03×10^{-15}, 6.46×10^{-16}, 5.34×10^{-16}, 3.54×10^{-16}, 4.44×10^{-18}, and 3.08×10^{-18} W m^{-2} yr kg^{-1} for near-anhydrous synthetic air, 40 % O_2/60 % Ar, and ambient air containing 3.8, 5.2, 19.9, and 22.2 g m^{-3} H_2O, respectively. The corresponding GWP_{100} values were 1.15×10^{-2}, 7.21×10^{-3}, 5.96×10^{-3}, 3.95×10^{-3}, 4.96×10^{-5}, and 3.44×10^{-5} for the same sequence of gas matrices (**Table 3**).

Within the ambient-air experiments, GWP_{100} decreased systematically with increasing humidity because the measured CF_3OF persistence became shorter. A shorter lifetime reduces the time-integrated radiative forcing and yields a smaller $f(\tau)$, representing the more spatially restricted atmospheric distribution expected for a rapidly removed compound. Thus, although CF_3OF exhibits appreciable infrared absorption and RE per unit atmospheric abundance, its cumulative direct radiative forcing is strongly limited by its short persistence under the investigated conditions.

The reported $AGWP_{100}$ and GWP_{100} values incorporate the lifetime-dependent distribution correction and should therefore be interpreted as condition-specific experimental evaluations. The measured CF_3OF decay times fall within the stated applicability range of the OH-type parameterization ($10^{-4} < \tau < 10^4$ years) but lie near its lower limit, where the correction is particularly approximate and may depend strongly on the location and conditions of emission (Hodnebrog et al., 2013, 2020). Moreover, this parameterization was developed for compounds removed primarily through reaction with tropospheric OH, whereas the CF_3OF decay observed here was strongly dependent on the water-vapor abundance and composition of the gas matrix. The lifetime-dependent parameterization was used to account for the restricted atmospheric distribution of short-lived CF_3OF; its application does not imply that reaction with OH is the dominant removal mechanism. The gas-cell e-folding times provide experimentally constrained measures of CF_3OF persistence under controlled near-surface conditions rather than independently determined global atmospheric lifetimes. Nevertheless, the consistently short decay times observed across all investigated matrices indicate that prolonged atmospheric accumulation of CF_3OF is unlikely.

Taken together, the consistently short decay times across the investigated gas matrices provide experimental constraints on the near-surface atmospheric persistence of CF_3OF. The resulting direct GWP_{100} values ranged from 3.44×10^{-5} to $1.15 \times$

https://doi.org/10.5194/egusphere-2026-6185
Preprint. Discussion started: 16 November 2026
© Author(s) 2026. CC BY 4.0 License.

10^{-2}, with the highest value obtained under the driest condition. These results demonstrate that the direct climate impact of CF_3OF is strongly limited by its short, condition-dependent persistence.

Table 3. Experimentally determined e-folding decay time, τ, lifetime-dependent distribution factor, $f(\tau)$, distribution-adjusted mass-based RE, $f(\tau) \times RE_{mass}$, $AGWP_{100}$, and GWP_{100} of CF_3OF under the investigated gas conditions. The mass-based RE was 5.86×10^{-12} W m^{-2} kg^{-1} for all conditions. $AGWP_{100}$ was calculated according to Eq. (9), and GWP_{100} was obtained using the reference $AGWP_{100}$ of CO_2, 8.95×10^{-14} W m^{-2} yr kg^{-1} (Smith et al., 2021). The whole-minute decay times in **Table 2** were converted to years using 1 yr = 365 days. AGWP and GWP calculations used the reported RE value of 0.108 W m^{-2} ppb^{-1}, derived values are rounded for presentation.

Sample type	τ (years)	$f(\tau)$	Distribution-adjusted RE (W m^{-2} kg^{-1})	$AGWP_{100}$ for CO_2 (W m^{-2} yr kg^{-1})	$AGWP_{100}$ (W m^{-2} yr kg^{-1})	GWP_{100}
Synthetic air (21 % O_2/N_2)	6.57×10^{-3}	0.02674	1.57×10^{-13}	8.95×10^{-14}	1.03×10^{-15}	1.15×10^{-2}
40 % O_2/60 % Ar	5.14×10^{-3}	0.02142	1.25×10^{-13}	8.95×10^{-14}	6.46×10^{-16}	7.21×10^{-3}
Ambient air 3.8 g m^{-3} H_2O	4.66×10^{-3}	0.01956	1.15×10^{-13}	8.95×10^{-14}	5.34×10^{-16}	5.96×10^{-3}
Ambient air 5.2 g m^{-3} H_2O	3.76×10^{-3}	0.01607	9.41×10^{-14}	8.95×10^{-14}	3.54×10^{-16}	3.95×10^{-3}
Ambient air 19.9 g m^{-3} H_2O	3.86×10^{-4}	0.00196	1.15×10^{-14}	8.95×10^{-14}	4.44×10^{-18}	4.96×10^{-5}
Ambient air 22.2 g m^{-3} H_2O	3.20×10^{-4}	0.00164	9.63×10^{-15}	8.95×10^{-14}	3.08×10^{-18}	3.44×10^{-5}

4. Conclusion

This study provides an experimentally based assessment of the infrared radiative properties, near-surface atmospheric persistence, and direct GWP_{100} of CF_3OF. To our knowledge, it presents the first quantitative gas-phase infrared ACS spectrum of CF_3OF suitable for RE calculations. The spectrum was dominated by structured absorption within 1167–1305 cm^{-1}, and the integrated ACS over 833.5–3000 cm^{-1} was 1.25×10^{-16} cm $molecule^{-1}$. Weighting the measured spectrum with the stratospheric-adjusted Pinnock curve yielded a mixing-ratio-based RE of 0.108 W m^{-2} ppb^{-1}. These results demonstrate that CF_3OF has appreciable radiative strength per unit atmospheric abundance and that its low climate impact cannot be attributed to weak infrared absorption alone.

Time-resolved FT-IR measurements showed that CF_3OF had short, condition-dependent persistence in all investigated gas matrices. The e-folding decay time was 3451 min in near-anhydrous synthetic air, decreased to 2704 min in the 40 % O_2/60 % Ar matrix, and ranged from 2448 to 168 min across the investigated ambient-air humidity conditions. Water vapor exerted the strongest observed influence on CF_3OF persistence, while increased O_2 abundance also accelerated its removal. In near-anhydrous synthetic air, the CO_2 rise time of 3591 min agreed with the CF_3OF decay time to within 4.1 %, providing kinetic evidence that CF_3OF loss was associated with CO_2 formation. Although a unique conversion mechanism could not be resolved, the coupled temporal behavior demonstrates that CF_3OF-derived carbon was converted to CO_2 with no spectral features attributable to COF_2 or other intermediates observed during the measurements.

Combining the measured RE with the condition-specific decay times and lifetime-dependent atmospheric-distribution correction yielded direct GWP_{100} values ranging from 3.44×10^{-5} to 1.15×10^{-2}, with the highest value obtained under the driest condition. Although the gas-cell decay times do not represent independently determined global atmospheric lifetimes,

https://doi.org/10.5194/egusphere-2026-6185
Preprint. Discussion started: 16 November 2026
© Author(s) 2026. CC BY 4.0 License.

their consistently short values across compositionally distinct matrices provide experimental constraints on the near-surface persistence of CF_3OF. The results therefore demonstrate that the appreciable RE of CF_3OF is offset by its rapid removal, strongly limiting its cumulative direct radiative forcing under the investigated conditions. Together with its reported plasma-processing capability (Kim et al., 2025), these findings support further consideration of CF_3OF as a promising low-GWP alternative to conventional high-GWP F-gases, subject to complementary evaluation of process performance, safety, degradation products, and overall life-cycle emissions.

Data availability

The data supporting the findings of this study, including infrared absorption cross-sections, CF_3OF decay measurements, CO_2 growth measurements, and GWP calculations, are available from Zenodo at https://doi.org/10.5281/zenodo.23045582 (Kim, 2026).

Author contributions

DK conceived and planned the study, designed the experiments, built the experimental apparatus, and coordinated and managed the day-to-day implementation of the research. DK and HK performed the experiments, interpreted the results, and contributed to manuscript writing. DK and HK share first authorship. HKP synthesized and supplied CF_3OF. BJ and SJH administered the research project, provided resources, supervised the experimental work, and contributed to manuscript review and revision in their supervisory roles.

Competing interests

The authors declare that they have no conflict of interest.

Financial support

This work was supported by the Technology Innovation Program (grant no. RS-2023-00266568), funded by the Ministry of Trade, Industry and Energy (MOTIE, Republic of Korea) and administered by the Korea Planning & Evaluation Institute of Industrial Technology (KEIT).

References

Allison, J. A. C. and Cady, G. H.: Reactions of Trifluoromethyl Hypofluorite with Organic Compounds, J. Am. Chem. Soc., 81, 1089–1091, https://doi.org/10.1021/ja01514a018, 1959.

An, S. and Hong, S. J.: Spectroscopic Analysis of NF_3 Plasmas with Oxygen Additive for PECVD Chamber Cleaning, Coatings, 13, 91, https://doi.org/10.3390/coatings13010091, 2023.

Aymonino, P. J.: The C–F stretching bands of trifluoromethoxyl fluoride (CF_3OF), J. Inorg. Nucl. Chem., 27, 2675–2676, https://doi.org/10.1016/0022-1902(65)80173-7, 1965.

dos Santos Afonso, M. and Schumacher, H. J.: Kinetics and the mechanism of the thermal reaction between trifluoromethylhypofluorite and hexafluoropropene, Int. J. Chem. Kinet., 16, 103–115, https://doi.org/10.1002/kin.550160203, 1984.

dos Santos Afonso, M., Romano, R. M., Della Védova, C. O., and Czarnowski, J.: Kinetics and mechanism of thermal gas-phase oxidation of hexafluoropropene in the presence of trifluoromethylhypofluorite, CF_3OF, Phys. Chem. Chem. Phys., 2, 1393–1399, https://doi.org/10.1039/a908989f, 2000.

https://doi.org/10.5194/egusphere-2026-6185
Preprint. Discussion started: 16 November 2026
© Author(s) 2026. CC BY 4.0 License.



Francisco, J. S.: A study of the gas-phase reaction of carbonyl fluoride with water, J. Atmos. Chem., 16, 285–292, https://doi.org/10.1007/bf00696901, 1993.

Harrison, J. J.: New infrared absorption cross sections for the infrared limb sounding of sulfur hexafluoride (SF_6), J. Quant. Spectrosc. Radiat. Transfer, 254, 107202, https://doi.org/10.1016/j.jqsrt.2020.107202, 2020.

Hodnebrog, Ø., Etminan, M., Fuglestvedt, J. S., Marston, G., Myhre, G., Nielsen, C. J., Shine, K. P., and Wallington, T. J.: Global warming potentials and radiative efficiencies of halocarbons and related compounds: A comprehensive review, Rev. Geophys., 51, 300–378, https://doi.org/10.1002/rog.20013, 2013.

Hodnebrog, Ø., Aamaas, B., Fuglestvedt, J. S., Marston, G., Myhre, G., Nielsen, C. J., Sandstad, M., Shine, K. P., and Wallington, T. J.: Updated Global Warming Potentials and Radiative Efficiencies of Halocarbons and Other Weak Atmospheric Absorbers, Rev. Geophys., 58, e2019RG000691, https://doi.org/10.1029/2019rg000691, 2020.

Kim, D.: Data for "Quantifying the Global Warming Potential of Trifluoromethyl Hypofluorite (CF_3OF): Infrared Absorption Cross-Sections and Decay Measurements", Zenodo [data set], https://doi.org/10.5281/zenodo.23045582, 2026.

Kim, D., Park, H. K., and Lee, J.: Experimental Determination of the Global Warming Potential of Carbonyl Fluoride (COF_2), Atmos. Chem. Phys., 26, 2707–2719, https://doi.org/10.5194/acp-26-2707-2026, 2026.

Kim, K. L., Hong, J. W., Jeon, Y. W., Jeong, J. W., Kim, C. H., Eoh, H. J., Kim, S. H., Park, J. S., Cho, N. I., Kwak, J. H., Kim, Y., and Yeom, G. Y.: Effect of $C_2H_2F_4/CF_4O$ with low global warming potentials on SiNx etching as a CHF_3 replacement, Sci. Rep., 15, 40517, https://doi.org/10.1038/s41598-025-24378-w, 2025.

Kurylo, M. J. and Orkin, V. L.: Determination of Atmospheric Lifetimes via the Measurement of OH Radical Kinetics, Chem. Rev., 103, 5049–5076, https://doi.org/10.1021/cr020524c, 2003.

Lagemann, R. T., Jones, E. A., and Woltz, P. J. H.: The Infrared and Raman Spectra of CF_3OF, J. Chem. Phys., 20, 1768–1771, https://doi.org/10.1063/1.1700286, 1952.

Lugani, G. S., Skaggs, R., Morris, B., Tolman, T., Tervo, D., Uhlenbrock, S., Hacker, J., Seng Tan, C., Nehlsen, J. P., Ridgeway, R. G., Wong Broadway, L., and Rudy, F. P.: Direct Emissions Reduction in Plasma Dry Etching Using Alternate Chemistries: Opportunities, Challenges, and Need for Collaboration, IEEE Trans. Semicond. Manuf., 37, 445–452, https://doi.org/10.1109/tsm.2024.3444465, 2024.

Myhre, G., Shindell, D., Bréon, F.-M., Collins, W., Fuglestvedt, J., Huang, J., Koch, D., Lamarque, J.-F., Lee, D., Mendoza, B., Nakajima, T., Robock, A., Stephens, G., Takemura, T., and Zhang, H.: Anthropogenic and Natural Radiative Forcing, in: Climate Change 2013: The Physical Science Basis. Contribution of Working Group I to the Fifth Assessment Report of the Intergovernmental Panel on Climate Change, edited by: Stocker, T. F., Qin, D., Plattner, G.-K., Tignor, M., Allen, S. K., Boschung, J., Nauels, A., Xia, Y., Bex, V., and Midgley, P. M., Cambridge University Press, Cambridge, UK and New York, NY, USA, 659–740, https://doi.org/10.1017/CBO9781107415324.018, 2013.

Pinnock, S., Hurley, M. D., Shine, K. P., Wallington, T. J., and Smyth, T. J.: Radiative forcing of climate by hydrochlorofluorocarbons and hydrofluorocarbons, J. Geophys. Res. Atmos., 100, 23227–23238, https://doi.org/10.1029/95jd02323, 1995.

Porter, R. S. and Cady, G. H.: Trifluoromethyl Hypofluorite: Its Decomposition and its Reaction with Carbonyl Fluoride to Form Perfluorodimethyl Peroxide, J. Am. Chem. Soc., 79, 5628–5631, https://doi.org/10.1021/ja01578a013, 1957.

Ravishankara, A. R., Solomon, S., Turnipseed, A. A., and Warren, R. F.: Atmospheric Lifetimes of Long-Lived Halogenated Species, Science, 259, 194–199, https://doi.org/10.1126/science.259.5092.194, 1993.

https://doi.org/10.5194/egusphere-2026-6185
Preprint. Discussion started: 16 November 2026
© Author(s) 2026. CC BY 4.0 License.



Shine, K. P. and Myhre, G.: The Spectral Nature of Stratospheric Temperature Adjustment and its Application to Halocarbon Radiative Forcing, J. Adv. Model. Earth Syst., 12, e2019MS001951, https://doi.org/10.1029/2019ms001951, 2020.

Smardzewski, R. R. and Fox, W. B.: Raman spectra of trifluoromethyl hypofluorite and hypochlorite in argon matrices at 8°K, J. Fluorine Chem., 6, 417–425, https://doi.org/10.1016/s0022-1139(00)81682-6, 1975.

Smith, C., Nicholls, Z. R. J., Armour, K., Collins, W., Forster, P., Meinshausen, M., Palmer, M. D., and Watanabe, M.: The Earth's Energy Budget, Climate Feedbacks, and Climate Sensitivity Supplementary Material, in: Climate Change 2021: The Physical Science Basis. Contribution of Working Group I to the Sixth Assessment Report of the Intergovernmental Panel on Climate Change, edited by: Masson-Delmotte, V., Zhai, P., Pirani, A., Connors, S. L., Péan, C., Berger, S., Caud, N., Chen, Y., Goldfarb, L., Gomis, M. I., Huang, M., Leitzell, K., Lonnoy, E., Matthews, J. B. R., Maycock, T. K., Waterfield, T., Yelekçi, O., Yu, R., and Zhou, B., https://www.ipcc.ch/report/ar6/wg1/downloads/report/IPCC_AR6_WGI_Chapter07_SM.pdf (last access: 28 September 2026), 2021.

Song, W. S., Kang, J. E., and Hong, S. J.: Spectroscopic Analysis of CF_4/O_2 Plasma Mixed with N_2 for Si_3N_4 Dry Etching, Coatings, 12, 1064, https://doi.org/10.3390/coatings12081064, 2022.

Sulbaek Andersen, M. P., Kyte, M., Andersen, S. T., Nielsen, C. J., and Nielsen, O. J.: Atmospheric Chemistry of $(CF_3)_2CF–C≡N$: A Replacement Compound for the Most Potent Industrial Greenhouse Gas, SF_6, Environ. Sci. Technol., 51, 1321–1329, https://doi.org/10.1021/acs.est.6b03758, 2017.

Trenberth, K. E. and Smith, L.: The Mass of the Atmosphere: A Constraint on Global Analyses, J. Climate, 18, 864–875, https://doi.org/10.1175/jcli-3299.1, 2005.

Uchimaru, T., Tsuzuki, S., Sugie, M., Tokuhashi, K., and Sekiya, A.: Ab initio study of the hydrolysis of carbonyl difluoride (CF_2O): importance of an additional water molecule, Chem. Phys. Lett., 396, 110–116, https://doi.org/10.1016/j.cplett.2004.08.022, 2004.

Wilt, P. M. and Jones, E. A.: New measurements of the vibrational spectrum of CF_3OF, J. Inorg. Nucl. Chem., 29, 2108–2109, https://doi.org/10.1016/0022-1902(67)80475-5, 1967.

Wilt, P. M. and Jones, E. A.: The vibrational spectra of CF_3OF, J. Inorg. Nucl. Chem., 30, 2933–2948, https://doi.org/10.1016/0022-1902(68)80153-8, 1968.

Yin, H.-M., Sun, J.-L., Li, Y.-M., He, G.-Z., and Han, K.-L.: A density function theory study on the properties and decomposition of CF_3OF, Chem. Phys. Lett., 356, 601–606, https://doi.org/10.1016/s0009-2614(02)00433-5, 2002.

Zachariah, M. R., Tsang, W., Westmoreland, P. R., and Burgess Jr., D. R. F.: Theoretical Prediction of the Thermochemistry and Kinetics of Reactions of CF_2O with Hydrogen Atom and Water, J. Phys. Chem., 99, 12512–12519, https://doi.org/10.1021/j100033a023, 1995.